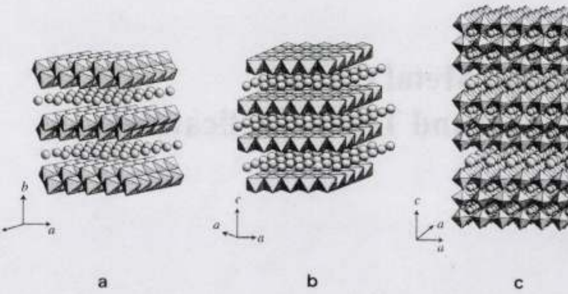

Figure 1. Crystal structures of layered host materials as a precursor of functional oxide Nnnosheets. (a) $Cs_{0.7}Ti_{1.825}\square_{0.175}O_4$ (□: vacancy), (b) $K_{0.45}MnO_2$, (c) $KCa_2Nb_3O_{10}$

Translucent colloidal suspensions were produced as a result of the reaction.

X-ray diffraction (XRD) study on a colloid centrifuged from the suspension indicated a high degree of swelling giving an intersheet separation of several nanometers or larger, as exemplified for the layered titanate, $H_{0.7}Ti_{1.825}\square_{0.175}O_4{\cdot}H_2O$ (Figure 2). Under a particular range of TBA concentration, sharp basal diffraction lines disappeared and were replaced by a broad profile. The other two layered materials also showed a broad pattern, which was characteristic of each host.[3,7,8] The broad profiles observed were very similar to the square of structure factor calculated based on a layer architecture of each compound. This agreement can be taken as strong evidence for the complete delamination, because the square of the structure factor should represent a profile based on X-ray scattering from independent oxide sheets. The sheets are not stacked in parallel to induce interference, but they are present as individual entities.

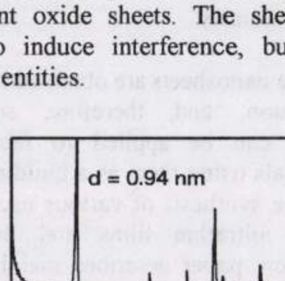

Figure 2. XRD patterns. (a) $H_{0.7}Ti_{1.825}\square_{0.175}O_4 \cdot H_2O$, (b) a colloid centrifuged from the suspension at $TBA^+/H^+ = 25$, (c) $TBA^+/H^+ = 2$. The sharp pattern in (a) indicates the orthorhombic layered structure of γ-FeOOH type. A broken trace in (c) represents the square of the structure factor, $F^2(0k0)$.

More direct evidence can be obtained by observations by transmission electron microscope (TEM) and atomic force microscope (AFM), which visualize sheet-like objects. The thickness estimated from AFM images was ~1.1 nm, ~0.8 nm, ~2.0 nm for the nanosheets of $Ti_{0.91}O_2$, $Ca_2Nb_3O_{10}$ and MnO_2, respectively, clearly demonstrating their unilamellar nature. Their lateral size generally reflected the original size of the precursor crystals, usually in a range of micrometers. Electron diffraction data collected from one sheet was composed of sharp spots, indicating the single-crystal quality.[9,10] The symmetry was compatible with that of the host layer in the precursors, indicating that the two-dimensional atomic arrangements remained basically unchanged.

PHYSICOCHEMICAL PROPERTIES

The nanosheets of $Ti_{0.91}O_2$ and $Ca_2Nb_3O_{10}$ showed semiconducting properties. For example, the $Ti_{0.91}O_2$ nanosheet generated photocurrent upon exposure to UV light. A detailed analysis of the action spectrum led to 3.8 eV as a bandgap energy, which is larger than that (3.2 eV) of bulk TiO_2 (anatase).[11] The larger bandgap may be ascribed to size-quantization effects. On the other hand, the MnO_2 nanosheet exhibited feasible redox capability. Manganese ions in the nanosheet can be electrochemically switched between 3+ and 4+ in response to a potential sweep.[12]

FABRICATION OF NANOSTRUCTURED MATERIALS USING NANOSHEETS AS A BUILDING BLOCK

The nanosheets were obtained as molecular entities dispersed in the colloidal suspension. They can be assembled or organized in various fashion to produce nanostructured materials by applying so-called wet-process synthetic techniques. In addition, they can be mixed with a range of foreign materials at a nanometer scale range to yield nanocomposites. We have reported the synthesis of various functional materials through these synthetic routes such as flocculation and layer-by-layer assembly.

Flocculation

Addition of electrolytes into the nanosheet suspension gave rise to restacking of the nanosheets trapping cationic species present in the solution. Lamellar nanocomposite materials can be easily synthesized through this approach. For example, rare earth (RE) ions can be incorporated between the gallery of $Ti_{0.91}O_2$ nanosheets simply by mixing the nanosheet suspension and a solution containing RE ions.[13] XRD measurement confirmed the formation of a lamellar structure (Figure 3). Two basal 0*k*0 peaks indicated a gallery height of 1.06 nm, which is compatible with the accommodation of hydrated RE ions. Two additional diffraction features at 2θ = 48° and 62° are attributable to the in-plane structure of the $Ti_{0.91}O_2$ sheet. Heavy doping of RE ions, ~10 mol%, was confirmed by chemical analysis. Note that direct intercalation into the bulk layered titanate cannot attain this high level of RE incorporation. The obtained restacked material showed intense characteristic emission from RE ions by exciting $Ti_{0.91}O_2$ nanosheets with UV light. The energy absorbed by the semiconducting nanosheets is

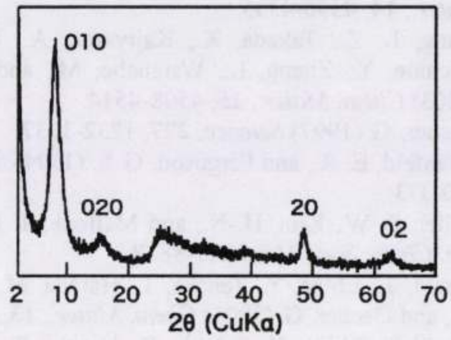

Figure 3. XRD pattern for a flocculated product of $Ti_{0.91}O_2$ nanosheets and Eu ions.

effectively transferred to excited states of 4*f* orbitals for RE ions, which relax to the ground state, emitting bright red light. The material had a higher thermal stability and mechanical strength in comparison with well-known RE complexes with organic ligands such as β-diketone.

Pillaring of layered materials with polyoxocations, e.g., aluminum Keggin ion, has been investigated extensively to convert them into microporous materials.[14,15] The synthetic route usually involves intercalation of polyoxocations into a layered compound followed by calcination at 400 – 500°C. In contrast to this conventional route, we recently found that restacking of the nanosheets with aluminum Keggin ions resulted in a new pillared structure, in which polyoxocations were arranged in double layers.[16,17] This unique structure enhanced the specific surface area and porosity in comparison with conventional materials with monolayer of pillars. The structure evolution may be understood by adsorption of polyoxocations on both sides of the nanosheets and subsequent aggregation of such a unit.

In addition to the examples above, the combination of nanosheets and cationic guest species can be designed to create a range of nanocomposites, which may be useful, for example, as a photocatalyst[18] and an electrode material.[19]

Layer-by-Layer Assembly

One of the most important achievements among material syntheses with nanosheets is the layer-by-layer deposition of the nanosheets to fabricate multilayer ultrathin films. A simple but powerful technique via sequential adsorption of oppositely charged species first developed by Decher for polymer films[20] is applicable to the oxide nanosheets, as first demonstrated with delaminated sheets of clay minerals and α-zirconium phosphate.[21,22] A multilayer assembly can be built up by alternately dipping a substrate in the colloidal suspension of nanosheets and an aqueous solution of cationic polymer, e.g., poly(diallyldimethylammonium) chloride (PDDA). Figure 4 depicts UV-visible absorption spectra in the buildup process of the multilayer film of $(Ti_{0.91}O_2/PDDA)_n$ on a quartz glass substrate.[23] The absorption peak at 265 nm is attributable to the $Ti_{0.91}O_2$ nanosheet. Its progressive enhancement with increasing the deposition cycle provided evidence for successful layer-by-layer deposition of the nanosheets. XRD measurements indicated the evolution of a Bragg peak having a spacing of 1.4 – 1.7 nm, which is attributable to a repeating nanostructure of inorganic nanosheet and organic

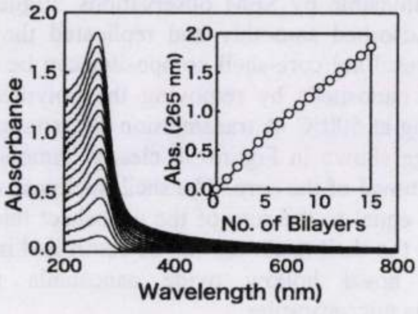

Figure 4. UV-visible absorption spectra in the course of multilayer buildup of $Ti_{0.91}O_2$ nanosheets /PDDA assembly. The inset shows the absorbance at 265 nm as a function of the number of bilayers.

polymer. Other characterizations by ellipsometry, FT-IR and AFM all provide support for the growth of multilayer nanocomposite films. This sequential adsorption procedure can control the thickness of ultrathin films with nanometer precision. The resulting composite films can be converted into inorganic films by removing polymer via heating and UV irradiation.[24] These ultrathin films are expected to have various applications depending on the consituent nanosheets and film architecture. For example, the films of $Ti_{0.91}O_2$ nanosheets may be useful as a UV-shielding or self-cleaning coating due to their high UV absorption capability and photochemical reactivity. Furthermore, we expect that the layer-by-layer procedure can be used to tailor superlattice-like assemblies with a complex structure, through which their function can be designed.

Recently Caruso et al. have reported the synthesis of core-shell particles by depositing nanoparticles onto micron-sized polymer beads via the LBL self-assembly procedure, and hollow shells by decomposing the polymer core.[25] One of the noteworthy features of the nanosheets is their highly flexible mechanical characteristics, making them ideal for shell buildup. They can cover spherical polymer beads like a wrapping paper.[26,27] Figure 5a shows scanning electron microscope (SEM) images of polystrene beads after coating with 20 bilayers of $Ti_{0.91}O_2$ nanosheet and cationic polymer. Although UV-visible and XRD data indicated successful multilayer buildup, the presence of the nanosheets

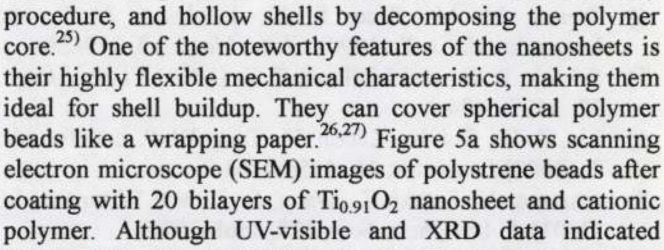

Figure 5. (a) SEM image for polystyrene beads coated with 20 bilayers of $Ti_{0.91}O_2$ nanosheets /PEI. (b) TEM image for hollow nanoshells obtained by heating the core/shell particles in (a) at 500°C.